

Tension variations of hydro-pneumatic riser tensioner and implications for dry-tree interface in semisubmersible

Hooi-Siang Kang¹, Moo-Hyun Kim^{*2} and Shankar S. Bhat Aramanadka³

¹Faculty of Mechanical Engineering, Universiti Teknologi Malaysia, Johor Bahru, Johor, Malaysia

²Department of Ocean Engineering, Texas A&M University, College Station, Texas, USA

³Sabah Shell Petroleum Co. Ltd., Kuala Lumpur, Malaysia

(Received November 24, 2016, Revised January 25, 2017, Accepted February 5, 2017)

Abstract. In real sea environments, excessive dynamic axial tension variations can be exerted on the top-tensioned risers (TTRs) and lead to structural integrity issues. The traditional riser-tension-variation analysis, however, by using parametric formulation is only conditionally valid under certain strict limits and potentially underestimates the total magnitudes of tension variations. This phenomenon is especially important for the long stroke tensioner in dry-tree semisubmersible with larger global heave motion and longer stroke. In this paper, the hydro-pneumatic tensioner (HPT) is modeled in detailed component-level which includes a set of hydraulic and pneumatic components. The viscous fluid frictional effect in the HPT is considered. The main objectives are (i) to develop a detailed tension variation model of the HPT; (ii) to identify the deviations between the conventional parametric formulation and component-level formulation; (iii) to numerically analyze the tension variation of long stroke tensioner in a dry-tree semisubmersible (DTS). The results demonstrate the necessity of component-level formulation for long stroke tensioner in the development of DTS.

Keywords: top-tension riser; hydro-pneumatic tensioner; tension variations; dry-tree semisubmersible

1. Introduction

The tensioner system of a top-tensioned riser (TTR) is designed to maintain a nearly constant axial tension on the contact point with the TTR so that the host platform is able to move relatively to the risers. The TTR must be tensioned so that the riser does not buckle under its own weight. The hydro-pneumatic tensioner (HPT) systems are a form of riser tensioning mechanism used to support TTRs on various dry-tree (well-head on deck) platforms. Conventionally, a plurality of hydraulic cylinders with hydro-pneumatic accumulators is connected between the platform and the riser to provide and maintain the necessary riser tension. Platform heave and horizontal motions causing hull set-down, necessitate changes in riser length relative to the platform, which causes the tensioning cylinders to stroke in (up-stroke) and out (down-stroke). The spring effect caused by the fluid compression or expansion during riser stroke partially isolates the riser from the low heave platform motions while maintaining a nearly constant riser tension. However, when the platform

*Corresponding author, Professor, E-mail: m-kim3@tamu.edu

takes a significant heave motion, the compression of the fluid in the cylinders causes increased cylinder pressure and thus increased riser tension (Crotwell and Yu 2011). The tension variations are important in the tensioner fatigue issues (Trent 2012) and sometimes can potentially be underestimated if only using the conventional parametric model (Gallagher *et al.* 2012).

In this paper, the formulation of riser tensioner is developed to identify the deviations in between the following two approaches in the marine tensioner-riser dynamic analysis: (i) parametric formulation (Yang 2009), and (ii) component-level formulation as the integrated component-level effects that considers the total component effects of the HPT (Kozik 1975, Kozik and Noerager 1976, Sten *et al.* 2010, Gallagher *et al.* 2012). The effects of dynamic tension variations acting on the TTR based on these two approaches are further simulated in a dry-tree semisubmersible (DTS) platform to identify the effects of tension variations caused by long stroke tensioner.

2. Hydro-Pneumatic Tensioner (HPT)

There are three most common types of tensioner systems in the offshore industry, categorized as wire-rope type, direct acting (pull-style), and ram-style (push-style), respectively. The wire-rope type had once been popular for decades in the offshore field developments. However, due to the complexity and limited payload ability of the wire-rope type system, the hydro-pneumatic (HP) types have become predominant in the more recent offshore field developments. The direct-acting (pull-style) tensioner and ram-style (push-style) tensioner can be further categorized as hydro-pneumatic (HP) tensioner. The direct-acting (pull-style) tensioners (DAT) are mounted with the piston rods looking down. Pressure applied to the rod side of the cylinders puts the piston rods in tension while pulling up on the riser to generate the riser tension (Crotwell and Yu 2011). The schematic diagram of hydro-pneumatic (HP) components is shown in Fig. 1 for a DAT system. The tensioner acts as heave compensating system that consists of a set of hydraulic-pneumatic system directly coupled to the riser at the tensioner ring attached to the slip joint (Sten *et al.* 2010). The tensioner cylinders are symmetrically mounted under the well deck. The tensioner cylinders are angled inboard to riser attachment points on a tensioner ring. The surface production tree or flow control device at the top of the riser on a host floating platform can be mounted closer to the tensioning point of the riser so that the well spacing inside the platform can be reduced. This reduces the bending loads induced in the portion of the riser above the tension point from the dynamic motions of the surface production equipment. Generally, the direct-acting tensioners (DATs) are designed for relatively short strokes and therefore this system is predominately utilized in tension-leg platform (TLP) due to the low heave characteristics of the hull, combined with the relatively small riser length changes associated with small heave motion and set down due to the parallelogram arrangement formed by the platform, tendons, risers, and the seafloor well pattern (Crotwell and Yu 2011).

On the other hand, the ram-style (push style) tensioners with long stroke are to be considered in the newly developed dry-tree semisubmersible concepts (Xiang *et al.* 2014). The discussion of the hydro-pneumatic system of a DAT tensioner can be generalized to the ram-style tensioner as well since that both systems are developed from the identical hydro-pneumatic principle. The main component is the tensioner cylinder that generates a pulling force (or pushing force in ram-style) on the tensioner ring. The pulling force (or pushing force) is generated by a hydro-pneumatic pressure in a closed volume. The cylinder of each tensioner is fluidly coupled, at its lower end (piston rod side) to a hydraulic fluid reservoir pressurized by a high pressure hydro-pneumatic accumulator.

hydraulic fluid from the tensioner cylinder to the accumulator (down stroke motion) during the extension of cylinder exerted large nonlinear air spring force caused by the compression of the air volume in the accumulator and pressure vessels. Due to the large dimensions of the tensioner system, the retracting and extending motions of tensioner cylinder involve large volumes of hydraulic-pneumatic flow. Therefore, a large volume of compressed nitrogen in the pressure vessels is necessary for reducing the pressure variations during this process (Sten *et al.* 2010).

3.1 Pressure variations in the nitrogen pressure vessel (NPV)

The high-pressure nitrogen pressure vessels (NPVs) are connected, by using pipes and hoses, to the accumulator under a constant preload pressure controlled by the nitrogen compressor as shown in Zone 1 in Fig. 1. The ball valves connected on these gas conduits are kept open during normal operation to maintain small tension variations (Grønevik 2013). The total gas volume in the boundary from the NPV to the gas domain inside the accumulator is regarded as single volume V_{A0} and the variation of gas volume change is represented by the volume ratio of $\Delta V_A/V_{A0}$. The local pressure variation in the high pressure NPV is a function of riser stroke length and that can be calculated when the internal area and initial pressure P_{A0} at the equilibrium mid-position are known. The upstroke/down-stroke motions of the tensioner rod give changes of volume in the oil/nitrogen accumulator and NPV. The change of volume ΔV_A is assumed as an adiabatic process (without the change of heat in between the system and its environment) (Grønevik 2013). The pressure variation ΔP_A in the high pressure gas domain (from NPV to accumulator) due to the variation of gas volume can be represented as (Kozik 1975)

$$\Delta P_A = P_{A0} \left(\left(1 - \Delta V_A / V_{A0} \right)^{-\gamma} - 1 \right) \quad (1)$$

where P_{A0} is the initial pressure in the high pressure NPV and γ is adiabatic gas constant, which is 1.4 of nitrogen at 15°C (Li *et al.* 2013). The decrement of volume $-\Delta V_A$ (compression of high pressure NPV gas domain during down-stroke motion) leads to the increment of pressure variation ΔP_A in the high pressure NPV (gas bank).

3.2 Pressure variations from NPV to accumulator

The high-pressure nitrogen pressure vessels (NPVs) are located at a certain distance away from the accumulator on the production / drilling deck (10 m, for instance) (Sten *et al.* 2010) and to be connected in gas flow connection through the pipes and valves, as illustrated in Zone 2 of Fig. 1. The frictional losses ΔP_{pt}^{HA} can occur as fluid (nitrogen in this case) moves through the pipes and conduits at a flow rate q_{gas}^{HA} and lead to the variations in pressure applied by the tensioner system. The pressure variations caused by the flow friction in the pipes and conduits is modeled by using Darcy-Weisbach equation (Manring 2005). This model is derived with the assumptions that the fluid/gas flow is fully developed along the pipe length and the effects due to the fluid/gas inertia and fluid/gas compressibility are not taken into account, which imply that features such as water hammer and the end effects of piping are not considered in this steady state fluid momentum conditions (Mathworks 2009). In order to account for local resistances, such as bends, fittings, inlet and outlet losses, and so on, all the resistances are converted into their equivalent lengths L_{eq}^{HA} , and then the total length of all the resistances is added to the pipe geometrical length L^{HA} . Therefore, the flow

pressure losses ΔP_{pl}^{HA} attributed by the pipes friction, according to Darcy-Weisbach equation, are defined as

$$\Delta P_{pl}^{HA} = \frac{\rho_{gas} f^{HA}}{2A_{HA}^2} \left(\frac{L^{HA} + L_{eq}^{HA}}{D_{HA}} \right) q_{gas}^{HA} \cdot |q_{gas}^{HA}| \quad (2)$$

where ρ_{gas} is the density of gas, while f^{HA} , A_{HA} , and D_{HA} are the friction factor, cross sectional area, and diameter of the pipe from the high pressure NPV (superscript H) to the accumulator (superscript A), respectively.

Pressure losses due to friction are proportional to the flow regime-dependable friction factor f^{HA} and the square of the flow rate q_{gas}^{HA} . The friction factor f^{HA} in Eq. (2) can be calculated based on Moody diagram by using the Haaland equation (Haaland 1983, Mathworks 2009) as shown in Eq. (3)

$$f^{HA} = \begin{cases} K_S / \text{Re} & \text{for } \text{Re} \leq \text{Re}_L \\ f_L + \frac{f_T - f_L}{\text{Re}_T - \text{Re}_L} (\text{Re} - \text{Re}_L) & \text{for } \text{Re}_L < \text{Re} < \text{Re}_T \\ \left\{ -1.8 \log_{10} \left(\frac{6.9}{\text{Re}} + \left(\frac{r_{hHA}}{3.7 D_{HA}} \right)^{1.11} \right) \right\}^{-2} & \text{for } \text{Re} \geq \text{Re}_T \end{cases} \quad (3)$$

$$\text{Re} = \frac{q_{gas}^{HA} \cdot D_{HA}}{A_{HA} v_{gas}} \quad (4)$$

where K_S is the shape factor that characterizes the pipe cross section, Re is the Reynolds number, f_L and f_T are friction factor at laminar border and turbulent border, respectively, Re_L and Re_T are maximum Reynolds number at laminar flow and turbulent flow, respectively, r_{hHA} is the height of the internal surface roughness on the pipe from the high pressure NPV (subscript H) to the accumulator (subscript A), and v_{gas} is the kinematic viscosity of nitrogen gas. It is noteworthy that the ball valves on the conduits from the NPVs to the accumulator in this paper are assumed to be fully opened and have the same flow diameter with the pipes in connection during the normal operation.

The preload pressure in the accumulator P_{pr} after considering the total effects of pressure variation ΔP_A in the high pressure NPV and pressure losses ΔP_{pl}^{HA} due to the pipeline and valve flow friction, as represented from the combination of Eq. (1) and Eq. (2), is stated as

$$P_{pr} = P_{A_0} + \Delta P_A + \Delta P_{pl}^{HA} \quad (5)$$

$$P_{pr} = P_{A_0} \left(1 - \Delta V_A / V_{A_0} \right)^{-\gamma} + \frac{\rho_{gas} f^{HA}}{2A_{HA}^2} \left(\frac{L^{HA} + L_{eq}^{HA}}{D_{HA}} \right) q_{gas}^{HA} \cdot |q_{gas}^{HA}| \quad (6)$$

3.3 Pressure variations from accumulator to the piston

In the hydro-pneumatic (HP) tensioner system, the accumulator consists of a pre-charged gas domain (which is connected to the high pressure NPVs) and a fluid domain (which is connected to the hydraulic part in the tensioner cylinder), as illustrated in Zone 3 of Fig. 1. If the hydraulic fluid pressure at the accumulator inlet P_{inlet} becomes higher than the preload pressure P_{pr} , which is acting on the gas-oil interface boundary, the hydraulic oil enters the accumulator chamber and compresses the gas domain, thus storing hydro-pneumatic energy. On the other hand, a drop in the inlet fluid pressure P_{inlet} during riser up-stroke motion restores the hydraulic oil back into the tensioner cylinder. The flow rate of hydraulic oil q_{oil} flow in / out the accumulator is calculated by using the fluid volumetric changes induced by the motion of tensioner piston. The shut-off valve on the conduit from the accumulator to the tensioner cylinder in this paper is assumed to be initially fully opened and has the same passage diameter with the pipes in connection during the normal operation. Therefore, the pressure at the piston-side chamber p_p^a after considering the pressure variation ΔP_A in high pressure NPV, pressure variation from the high pressure NPV to the accumulator ΔP_{pl}^{HA} , and pressure losses ΔP_{pl}^{AP} due to the pipe friction and valve flow friction can be represented as

$$P_p^a = P_{pr} + \Delta P_{pl}^{AP} \quad (7)$$

$$P_p^a = P_{A_0} + \Delta P_A + \Delta P_{pl}^{HA} + \Delta P_{pl}^{AP} \quad (8)$$

$$P_p^a = P_{A_0} \left(\frac{1}{(1 - \Delta V_A / V_{A_0})^\gamma} \right) + \frac{\rho_{gas} f^{HA}}{2A_{HA}^2} \left(\frac{L^{HA} + L_{eq}^{HA}}{D_{HA}} \right) q_{gas}^{HA} \cdot |q_{gas}^{HA}| \quad (9)$$

$$+ \frac{\rho_{oil} f^{AP}}{2A_{AP}^2} \left(\frac{L^{AP} + L_{eq}^{AP}}{D_{AP}} \right) q_{oil} \cdot |q_{oil}|$$

where ρ_{oil} is the density of hydraulic oil, q_{oil} is the flow rate of hydraulic oil, f^{AP} , A_{AP} , and D_{AP} are the friction factor, cross sectional area, and diameter of the pipe from the accumulator (superscript A) to the tensioner piston (superscript P), respectively. The method to calculate the oil friction factor f^{AP} is the same as the gas friction factor f^{HA} in the Eq. (3), by modifying the Reynold number in Eq. (4) for the corresponding hydraulic oil inputs.

In general, the pressure loss ΔP_{pl}^{HA} due to the friction of gas is around three orders of magnitudes smaller than the liquid ΔP_{pl}^{AP} , in the case of nitrogen/oil, due to the density of the fluid (Van de Ven and Li 2009). Hence, Eq. (9) can be simplified, under a reasonable level of accuracy, into

$$P_p^a \approx P_{A_0} (1 - \Delta V_A / V_{A_0})^{-\gamma} + \frac{\rho_{oil} f^{AP}}{2A_{AP}^2} \left(\frac{L^{AP} + L_{eq}^{AP}}{D_{AP}} \right) q_{oil} \cdot |q_{oil}| \quad (10)$$

The industrial practices normally assume that the frictional losses of hydraulic oil in between the accumulator and the tensioner cylinder, which is the second term of the right hand side of Eq. (10), are to be neglected (Yang 2009). Therefore, Eq. (10) is further simplified, as the parametric formulation, into

$$P_p^a \approx P_{A_0} \left(\frac{1}{(1 - \Delta V_A / V_{A_0})^\gamma} \right) \quad (11)$$

The Eq. (11) is solely dependent on the pneumatic effects in the hydro-pneumatic tensioner (HPT). The pressure at the piston-side chamber p_p^a is highly dependable with respect to the ratio of volume change in the gas domain $\Delta V_A/V_{A0}$ and the gas constant γ . The Eq. (11) can be rewritten into the form of tension force T exerted from the tensioner cylinder piston as in the following equation (Yang 2009, Kang 2015)

$$T = T_0 \left(1 - \frac{\Delta z}{z_0} \right)^{-\gamma} \quad (12)$$

where T_0 is the pretension of tensioner, z_0 is the equivalent length of cylinder (which is the ratio of total fluid volume to cylinder piston-side cross-sectional area), and Δz is the change of platform-riser relative displacement.

The parametric formulation in Eq. (12) is reasonable if the length of connection pipes L^{AP} is sufficiently short (Trent 2012) or the relative velocity of the platform-riser in the heave direction is sufficiently small, such as in the case of TLP. However, it is noteworthy that the hydraulic pressure losses ΔP_{pl}^{AP} through the pipes in between the accumulator and the piston in Eq. (10) must be evaluated if the velocity of riser stroke is sufficiently large, such as under the operations of drillship, dry-tree semisubmersible, and during the anti-recoiling and disconnection of TTR.

It is noteworthy that the formulation of Eq. (10) is based on the assumption that the fluid compressibility and leakages inside the tensioner cylinder are assumed to be negligible. Hence, the equation of force equilibrium on both sides of tensioner piston F_{ten} in the hydraulic-pneumatic cylinder can be represented as

$$F_{ten} = A_p^a \cdot P_p^a - A_p^b \cdot P_p^b + F_{HS} \quad (13)$$

$$\begin{aligned} F_{ten} = & F_{HP_0}^a \left(1 - \frac{\Delta z}{z_{A0}} \right)^{-\gamma} + A_p^a \cdot \frac{\rho_{oil} f^{AP}}{2A_{AP}^2} \left(\frac{L^{AP} + L_{eq}^{AP}}{D_{AP}} \right) q_{oil} \cdot |q_{oil}| \\ & - F_{HP_0}^b \left(1 + \frac{\Delta z}{z_{B0}} \right)^{-\gamma} + A_p^b \cdot \frac{\rho_{gas} f^{LP}}{2A_{LP}^2} \left(\frac{L^{LP} + L_{eq}^{LP}}{D_{LP}} \right) q_{gas}^{LP} \cdot |q_{gas}^{LP}| + F_{HS} \end{aligned} \quad (14)$$

where F_{HS} is the hard-stop force when the piston is approaching very closely the upper/lower limits of the cylinder, which can be modeled as a cubic spring force (Yang 2009), z_{A0} and z_{B0} are the total equivalent lengths of cylinder stroke in piston-side and cap-side, respectively, $F_{HP_0}^a$ and $F_{HP_0}^b$ are the initial forces acting on the piston at the piston-side and cap-side, respectively, A_p^a and A_p^b are the cross sectional areas of the piston at the piston-side and cap-side, respectively, A_{LP} and D_{LP} are the cross sectional area and diameter of the pipe, respectively, from the tensioner piston (subscript P) to the low pressure NPV (subscript L). Since the density of nitrogen is around three orders of magnitudes smaller than that of hydraulic oil (Van de Ven and Li 2009), the pressure losses due to the friction of gas can be neglected in Eq. (14) under a reasonable level of accuracy

$$F_{ten} \approx F_{HP_0}^a \left(1 - \frac{\Delta z}{z_{A0}} \right)^{-\gamma} + A_p^a \cdot \frac{\rho_{oil} f^{AP}}{2A_{AP}^2} \left(\frac{L^{AP} + L_{eq}^{AP}}{D_{AP}} \right) q_{oil} \cdot |q_{oil}| - F_{HP_0}^b \left(1 + \frac{\Delta z}{z_{B0}} \right)^{-\gamma} + F_{HS} \quad (15)$$

It is noteworthy that the third term in the right-hand-side of Eq. (15) is normally acting as an air

spring for the up-stroke motion and, in general, F_{HP0}^b which is connected to the low-pressure NPV, is much smaller than F_{HP0}^a .

4. Modeling of coupled dynamics of platform, riser and HPT under tension variations

The finite element (FE) model of the nonlinear HPT and the floating platform motion is implemented in CHARM3D, a fully-coupled time-domain dynamic-analysis program for floating bodies, mooring lines/tendons, and risers (Ran 2000, Koo *et al.* 2004, Yang and Kim 2011, Kang and Kim 2012, Bae and Kim 2013, Kang *et al.* 2013, Kang *et al.* 2014, Kim and Kim 2015). The frequency-dependent hydrodynamic coefficients and the first-order and second-order wave excitation forces and moments are calculated by the near-field method by using WAMIT (Lee and Newman 1991), a diffraction/radiation panel program. The corresponding forces are converted to the time-domain terms using a two-term Volterra series expansion in CHARM3D. The frequency-dependent radiation damping was included in the form of a convolution integral in the time domain simulation. Viscous forces are included through the drag force term in Morison's equation (Yang and Kim 2010).

A detailed modeling of coupled dynamics of floating platform and riser in CHARM3D can be found in the works of Ran (2000). In this paper, the effects of HPT's tension variations are included. By assuming that the low-pressure NPV is considerably lower pressurized than the high-pressure NPVs, the air-spring reaction force F_{HP0}^b on the cap-side is significantly smaller than the pulling force F_{HP0}^a from the piston-side, which is $F_{HP0}^a \gg F_{HP0}^b$, then the tension F_{ten} to be exerted by the hydro-pneumatic tensioner (HPT) can be approximated from Eq. (15) as

$$F_{ten} \approx F_{HP0} \left(1 - \frac{\Delta z}{z_0}\right)^{-\gamma} + A_a \cdot \frac{\rho_{oil} f^{AP}}{2} \left(\frac{L^{AP} + L_{eq}^{AP}}{D_{AP}}\right) v_{AP} \cdot |v_{AP}| \quad (16)$$

$$v_{AP} \cdot |v_{AP}| = v_z |v_z| \cdot \left(\frac{A_a}{A_{AP}}\right)^2 \quad (17)$$

where v_{AP} is the fluid velocity in the HPT connector pipe, and v_z is the velocity of piston in the HPT cylinder. By applying time-domain integration to Eq. (16) in the CHARM3D as derived in Kang (2015), the coupling terms of riser finite element tangential stiffness matrix that need to be added into the global stiffness matrix in CHARM3D after including tension variations can be represented as

$$\frac{\Delta t}{2} \left\{ \begin{array}{c} \left[\begin{array}{cccc} 0 & 0 & K_{ij}^{rx} & K_{ij}^{r\theta} \\ 0 & 0 & 0 & K_{ij}^{r'\theta} \\ K_{ij}^{xr} & 0 & 0 & 0 \\ K_{ij}^{\theta r} & K_{ij}^{\theta r'} & 0 & 0 \end{array} \right]_{LS} + \left[\begin{array}{cccc} 0 & 0 & K_{ij}^{rx} & K_{ij}^{r\theta} \\ 0 & 0 & 0 & 0 \\ K_{ij}^{xr} & 0 & 0 & 0 \\ K_{ij}^{\theta r} & 0 & 0 & 0 \end{array} \right]_{TV} \end{array} \right\} \begin{Bmatrix} \Delta r_j \\ \Delta r_j' \\ \Delta X_j \\ \Delta \theta_j \end{Bmatrix} = \frac{\Delta t}{2} \begin{Bmatrix} 2N_i \\ 2L_i \\ 2F_i \\ 2M_i \end{Bmatrix} + \frac{\Delta t}{2} \begin{Bmatrix} -2 \cdot n_{cyn} \cdot F_{HP_{dyn}} \\ 0 \\ 2 \cdot n_{cyn} \cdot F_{HP_{dyn}} \\ 0 \end{Bmatrix}_{TV} \quad (18)$$

where K_{ij}^{AB} are the coupling stiffness coefficients. In CHARM3D, the symbol K_{ij}^{AB} indicates that the tangential stiffness coefficient for degree of freedom B in the direction A . The subscription LS refers to the coupling connection between the floating platform and riser top node based on Eq. (12). On

the other hand, the subscription TV refers to the addition of tension variations on the coupling connection. Δt is time step of the numerical simulation, ΔX_j is the change of translational motion of the floating platform at its origin of the body coordinate system at each simulation step and $\Delta \theta_j$ is the change of angular motion of the floating platform at each simulation step. Also, Δr_j is the change of position of the riser top node which is connected to the floating platform and $\Delta r_j'$ is the change of tangent to the riser centerline at each simulation step. N_i is the nodal resultant force on the riser top node, F_i is the nodal resultant force acting on the floating platform, where $F_i = -N_i$. Moreover, L_i is nodal resultant moment on the riser top node, and M_i is the nodal resultant moment acting on the floating platform, where $M_i = L_i \times r_i'$ (Ran 2000). n_{cyn} is the total number of hydro-pneumatic cylinder of the riser tensioner, and F_{HPdyn} is the dynamic part of Eq. (16), which causes the frictional effects in the tensioner

$$F_{HPdyn} = A_a \cdot \frac{\rho_{oil} f^{AP}}{2} \left(\frac{L^{AP} + L_{eq}^{AP}}{D_{AP}} \right) v_{AP} \cdot |v_{AP}| \quad (19)$$

5. Numerical analyses of HPT tension variations in regular wave

In order to identify the deviations in between the parametric formulation (Eqs. (11)-(12)) and component-level formulation (Eq. (10) and Eq. (15)) in the analysis of TTR axial tension, the effects of dynamic pressure/tension variations on different numerical models of hydro-pneumatic tensioner (HPT) were investigated under the following two settings: (1) a nonlinear HPT was simulated under a dynamic stroke and velocity for regular wave (Fig. 2); (2) the length of hydraulic pipe was varied in order to simulate the pressure variations attributed by the frictional fluid effects (Figs. 3-5). The

Table 1 Hydraulic-pneumatic tensioner data

Pressure at LNPV*	10 bar
Volume of LNPV	4.0 m ³
Pressure at HPNV*	60 bar
Volume of HNPV	9.0 m ³
Length of pipe from LNPV to cylinder	30.0 m
Diameter of pipe from LNPV to cylinder	0.1 m
Length of pipe from HNPV to accumulator	30.0 m
Diameter of pipe from HNPV to accumulator	0.1 m
Length of pipe from accumulator to piston	Variable
Diameter of pipe from accumulator to cylinder	0.2 m
Cylinder inner diameter	0.560 m
Piston rod diameter	0.230 m
Density of hydraulic oil	850 kg/m ³
Viscosity of hydraulic oil	84.2416 cSt**

*LNPV=low pressure nitrogen pressure vessel, HNPV = high pressure nitrogen pressure vessel;

**1 cSt=1×10⁻⁶ m²/s

simulation was conducted by using the Simulink software package (Mathworks 2009) and the CHARM3D. The dimensions and data of HPT are tabulated in Table 1.

The characteristic responses of the hydro-pneumatic tensioner (HPT) are shown in Fig. 2. The tensioner was excited by a sinusoidal dynamic stroke Δz (from -0.50 m to 4.25 m, positive sign is referred to down-stroke motion) and dynamic velocity (from -1.0 m/s to 1.0 m/s) in this case. The velocity of the HPT's piston is normally far below 1.0 m/s when the host platform is the tension-leg platform (TLP). However, the dynamic velocity inputs in this simulation are reasonable for the cases of drillship and dry-tree semisubmersible, in which the platform heave motion is no longer constrained by the stiff tendons and for the case of instantaneous velocity during anti-recoiling and TTR disconnection. The position of piston after taking the overall static loadings into account is at around +2.0 m (positive sign is referred to downward direction in this case). If the dynamic loadings are included, it can be seen that the piston dynamic displacement and velocity are out of phase, with maximum velocity occurring as the piston reaches static equilibrium position (Sten *et al.* 2010). The pressure in the piston-side chamber, based on Eq. (9), has the phase in between the piston displacement and piston velocity.

The effects on the pressure variations in tensioner cylinder due to the frictional losses in the pipes are shown in Fig. 3. The contribution of frictional losses to the pressure variations is stated by the second term of the right hand side of Eq. (10). It can be found that the effects of friction for the 30 m length L^{AP} long pipe is significant compared to the one with 3 m short-length L^{AP} pipe. The percentage of dynamic pressure variation for long pipe is ~43% while the pressure variation for the short pipe is ~11%, with respect to mean pressure. The dynamic pressure (and tension) variations are very sensitive to the length of hydraulic fluid pipe in the HPT. Therefore, in order to reduce dynamic tension variations, the hydraulic pipe must be designed as short as possible, which means that the location of the accumulator and the tensioner cylinder is recommended to be as close as possible.

The validity and accuracy of the parametric formulation of HPT, as stated in Eq. (11) (Yang 2009, Yang and Kim 2010), was analyzed and shown in Fig. 4. The pressure variations of the 3 m short pipe were compared with the case that the frictional losses of hydraulic oil in between the accumulator and the tensioner cylinder ΔP_{pt}^{AP} are neglected. It is seen that the simplified

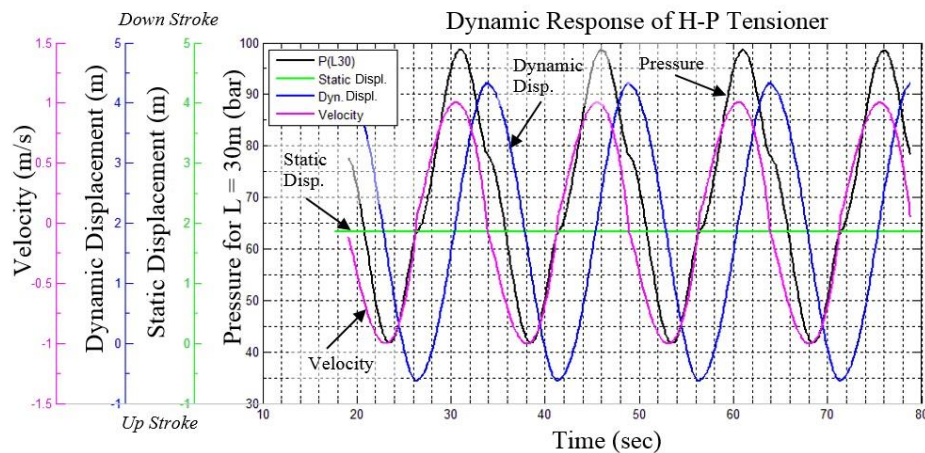


Fig. 2 Dynamic response of HP tensioner

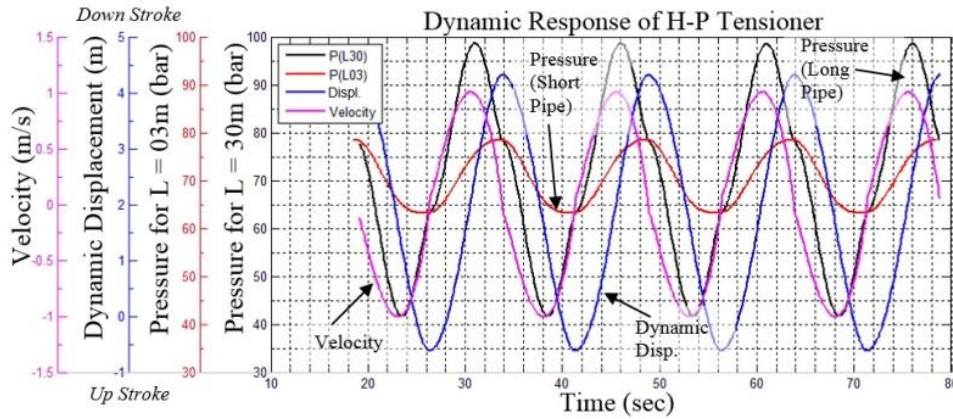


Fig. 3 Pressure variations due to the frictional losses in the pipes

parametric formulation is conditionally valid if the length of connection pipes L^{AP} is sufficiently short (3 m to 0 m), even though the dynamic velocity is large (~ -1.0 m/s to 1.0 m/s). Therefore, the accuracy of the parametric formulation (Eq. (11)), which is a popular riser tension analysis method in the industry, is very dependent on the physical length of the hydraulic pipe L^{AP} of the HPT system. The excessive dynamic tension variations are potentially to be underestimated if the HPT is built with long hydraulic conduits and long stroke. For instance, the long-stroke tensioner is used in the dry-tree semisubmersible.

The pressure-displacement and pressure-velocity plots with respect to the different lengths of pipes (or hydraulic fluid traveling length) are shown in Fig. 5. It is apparent that the pressure is a function not only of piston displacement but also of the piston velocity. Throughout the loops (in the clock-wise direction), the pressure is greater with the extension of tensioner cylinder (positive sign is referred to down-stroke motion in this case). The variations of hysteresis are smallest at two end points (at ~ -0.5 m and ~ 4.25 m, respectively) and are most pronounced at the static equilibrium point (which is at around $+2.0$ m in this case). It is noteworthy that the pressure variations are very dependable to the frictional length of pipe conduits. If the length of hydraulic flow pipe is sufficiently short (if L^{AP} very close to 0 m), as expressed in Eq. (11), the pressure-displacement loop is reduced to a curve line (the *blue* line in Fig. 5), which normally represents the HPT tension-stroke characteristics in the industrial manufacturer manuals.

6. Numerical simulation in irregular sea condition for semisubmersible with dry-tree interface

From the numerical analyses in the regular wave condition, it can be found that the tension variation of HPT is dependent on the length of hydraulic fluid traveling per cycle, and the relative velocity in between the platform and TTR. These two factors contribute minor effects in the TLP because the tensioners in TLP are short stroke with typically in the range from 6 ft (1.83 m) to 10 ft (3.05 m) (Leverette *et al.* 2013); hence the maximum allowable traveling length per cycle is small. Moreover, the relative velocity of TLP-TTR is much smaller than one in the semisubmersible platform. These two key factors in tension variations, however, become very significant in the

developments of dry-tree semisubmersible. The heave motion of typical dry-tree semisubmersible (DTS) is large and long stroke tensioner is required to compensate this heave motion. Zeng *et al.* (2013) proposed a deep-draft DTS comprising a two-axis symmetrical hull with draft in the range of 100 ft (30.48 m) to 155 ft (47.24 m) to accommodate the tensioner stroke in the range of 35 ft (10.67 m) to 45 ft (13.72 m). Poll *et al.* (2013) designed a Paired-Column Semisubmersible Hull (PC-Semi) with draft of 175 ft (53.34 m) to accommodate the tensioner stroke of 28 ft (8.53 m). In addition, Bian and Xiang (2013) also suggested a DTS hull with the draft of 150 ft (45.72 m) to support the tensioner stroke within 35 ft (10.67 m). From these reported data of the long stroke tensioner to be installed in the DTS, even if the accumulator is designed to be located just beside the cylinder (Trent 2012), the hydraulic fluid is allowed to flow from 8.53 m to 13.72 m inside the length of tensioner cylinder.

A generic type of DTS model with 12 chain-polyester-chain mooring lines, 4 steel catenary risers (SCRs), 2 dual-barrier top tension risers (TTRs) with top tension factor 1.34 is selected for the numerical analyses of tension variations in irregular sea condition. The principal dimensions of the

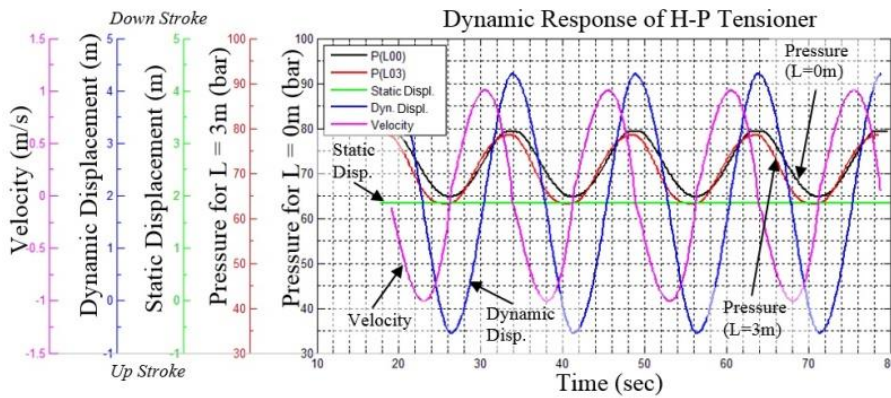


Fig. 4 Pressure variations due to the frictional pipe lengths

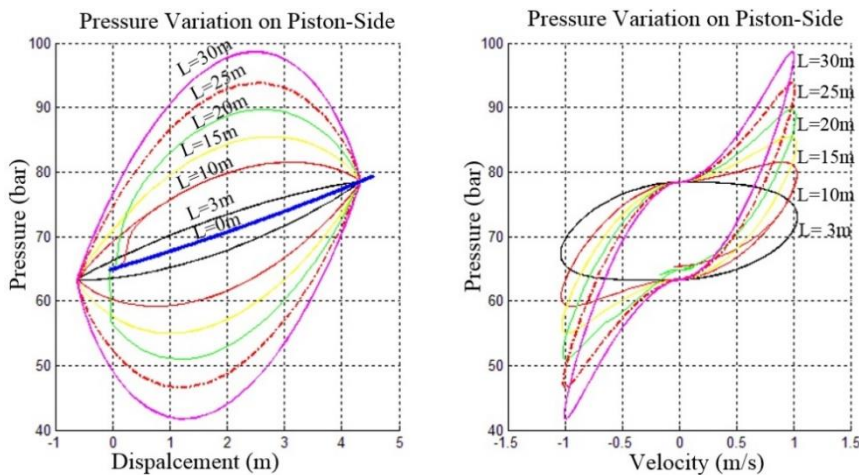


Fig. 5 Pressure variations in the piston-side chamber, positive stroke is referred to down-stroke motion in this case

DTS platform are tabulated in Table 2. The dimensions and data of HPT have been modified from Table 1, and tabulated in Table 3, to customize the DTS setting where the stiffness of long-stroke tensioner at zero-displacement is 54 kN/m. Three-hour time-simulations are carried out in a Central Gulf of Mexico (GOM) 100-year extreme environmental condition where the metocean profiles are listed in Table 4. Wave, wind, and current are collinear with 180° incident angle.

The time series of TTR's stroke in the simulation of DTS under irregular sea condition is shown in Fig. 6. The maximum down-stroke and maximum upstroke are -3.746 m and +5.713 m, respectively. The simulated tension-stroke curve at piston side chamber of a single cylinder in the

Table 2 Principal dimensions of the generic semisubmersible model

Water depth	1219.2 m
Number of column, pontoon	4, 4
Draft	28.96 m
Total weight	29840 ST (265470 kN)
Hull group	10928 ST (97220 kN)
Deck facility	10000 ST (88964 kN)
Drilling group	3000 ST (26689 kN)
Riser pretension at the top	2216 ST (19715 kN)
Mooring load	3624 ST (32241 kN)
Single BOP tree weight	20 kips (88.96 kN)
Displacement	34810 MT (309685 kN)

*ST=short ton, MT=metric ton; data from estimation and not related to any well-existed dry-tree semisubmersible

Table 3 Hydraulic-pneumatic tensioner data for DTS

Total number of cylinders	6
Pressure at LNPV	8.30 bar
Volume of LNPV	8.0 m ³
Pressure at HNPV	49.30 bar
Volume of HNPV	2.5 m ³
Length of pipe from LNPV to cylinder*	0.1 m
Diameter of pipe from LNPV to cylinder	0.1524 m
Length of pipe from HNPV to accumulator*	0.1 m
Diameter of pipe from HNPV to accumulator	0.1524 m
Length of pipe from accumulator to piston	10.0 m
Diameter of pipe from accumulator to cylinder	0.1524 m
Cross-sectional area of cylinder	0.2463 m ²
Hydraulic fluid area of piston-side	0.2048 m ²
Density of hydraulic oil	850 kg/m ³
Viscosity of hydraulic oil	84.2416 cSt

*to be negligible in long-stroke tensioner case

Table 4 Wave, current, and wind profiles of the central-GOM 100-year condition

Significant wave height, H_s		15.8 m
Peak period, T_p		15.4 s
Overshooting parameter, γ		2.40
Direction of waves and current (collinear)		180 deg
Current profile	Surface speed	2.40 m/s
	Speed at mid-profile	1.80 m/s
	Zero-speed depth	100.80 m
Wind	10 m elevation	48.00 m/s

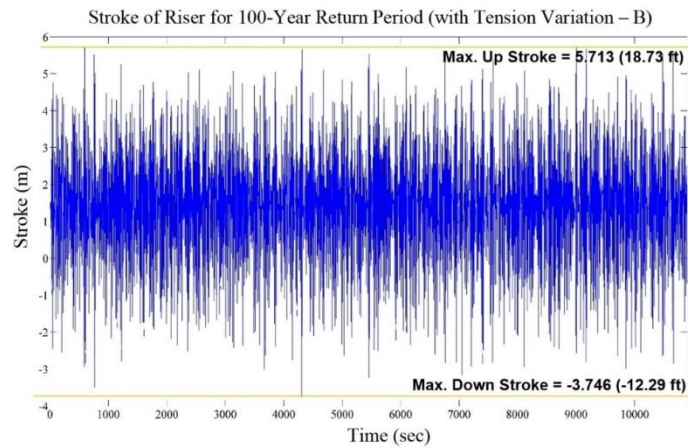


Fig. 6 Stroke of TTR interface with dynamic tension variations in DTS platform

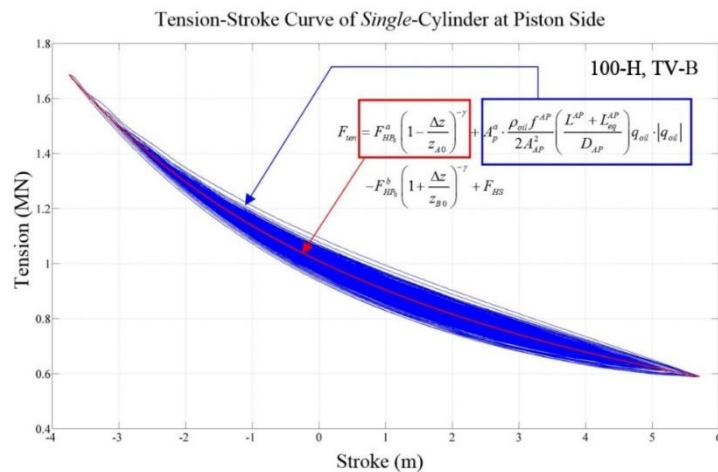


Fig. 7 Simulation of tension exerted in the piston-side chamber for single cylinder in the long-stroke tensioner (L=10 m) for dry-tree semisubmersible case

HPT is shown in Fig. 7. The tension is ranged in [~ 0.60 MN to ~ 1.70 MN]. The maximum allowable traveling length of the long-stroke tensioner is set to 10 m for the case of DTS under irregular sea

and extreme environmental conditions. The negative sign in the DTS case is referred to the down-stroke motion (which is different from the sign convention in the cases of regular wave simulation) for matching the DTS global coordinate system.

As shown in Fig. 8, the tension variations exerted in single HPT cylinder at its piston side varied from -9.0% to 11.0% from the parametric formulation results, after taking the hydraulic effects (the second term in Eq. (15)) into account. It can be inferred from the results in Fig. 5 and Eq. (15) that when the maximum allowable traveling length for long stroke cylinder is increased from 10 m to 13.72 m (45 ft) (Zeng *et al.* 2013), larger percentage of tension variations can be expected.

The tension variations in the piston-side chamber for single cylinder in the long-stroke tensioner ($L=10$ m) for dry-tree semisubmersible case with respect to variations of velocity is shown in Fig. 9. As expected from the Eq. (15), larger relative velocity in between the DTS and the TTR generates larger tension variations. The maximum velocity for DTS in this case varied from ~ -2.5 m/s to ~ 2.0 m/s. From the results in Figs. 6-9, it can be further inferred that the excessive tension variations are induced from the following sources and effects;

- The hydraulic fluid flow rate q_{oil} which is induced by the velocity of tensioner piston, as stated in Eq. (15). The larger tension variations caused by the larger velocity factor are reasonable for the cases of dry-tree semisubmersible (DTS), where the platform heave motions are no longer constrained by the stiff tendons.

- The geometrical dimension, especially the length of hydraulic pipe conduits L^{AP} , as stated in Eq. (15). The excessive tension variations will be exerted with longer hydraulic fluid travel between the accumulator and tensioner cylinder, such as in the case of long-stroke tensioner.

- The ratio of gas volume $\Delta V_A/V_{A0}$ between the displaced volume and the total gas volume stored in the high pressure NPVs, as stated in the Eq. (10) and Eq. (11). This volume ratio must be designed as small as possible to minimize the dynamic tension variations. Therefore, a very large volume V_{A0} of high pressure NPVs must be stored nearby the well bay. For the long-stroke tensioner to be developed in the dry-tree semisubmersible platform, the required storage of high-pressurized gas volume is even larger.

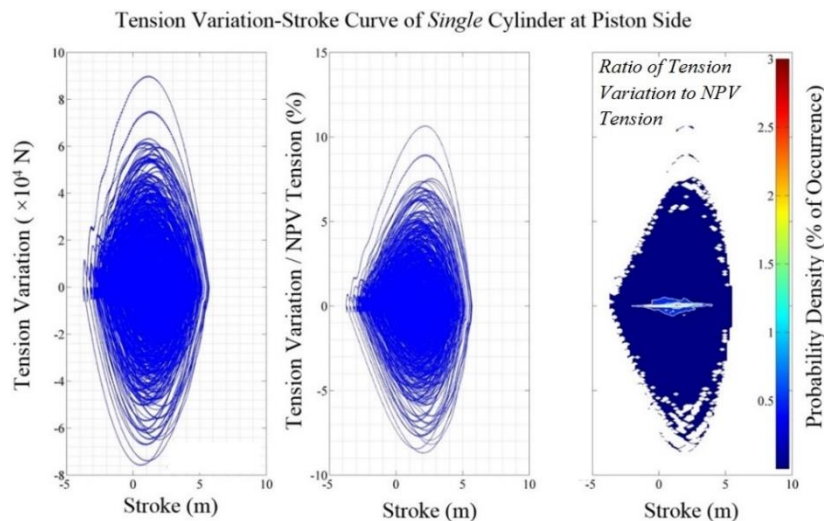


Fig. 8 Tension variations in the piston-side chamber for single cylinder in the long-stroke tensioner ($L=10$ m) for dry-tree semisubmersible case with respect to variations of stroke

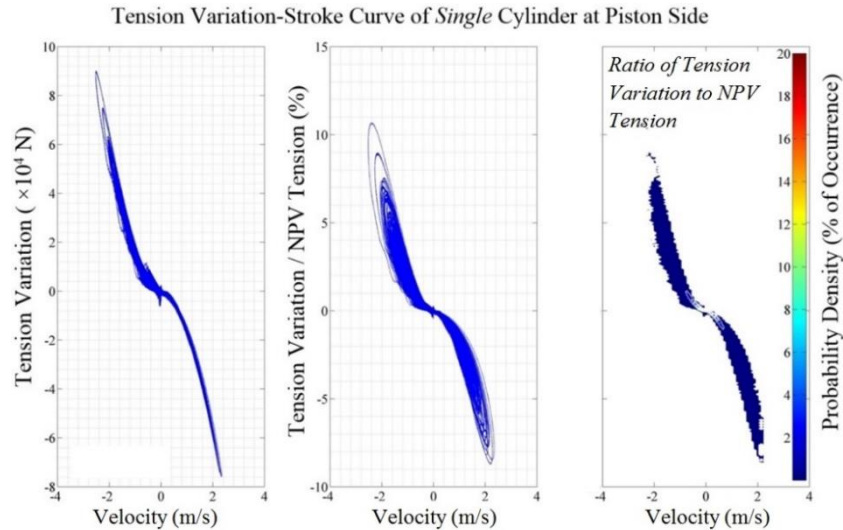


Fig. 9 Tension variations in the piston-side chamber for single cylinder in the long-stroke tensioner ($L=10$ m) for dry-tree semisubmersible case with respect to variations of velocity

7. Conclusions

In this paper, the formulation of riser tensioner is developed to identify the deviations from the simplified parametric formulation due to the integrated combined component-level effects. The excessive tension variations may potentially be under-estimated when using the conventional parametric model. The larger tension variations caused by the larger velocities are found in the case of dry-tree semisubmersible. The dynamic tension variations are also sensitive to the hydro-pneumatic system geometrical dimension, especially the lengths of hydraulic pipe conduits. It is concluded that a more comprehensive formulation of long-stroke tensioner is necessary to include the effects of excessive tension variations when the longer hydraulic fluid traveling length is required, such as the case of long-stroke HP tensioner in the development of dry-tree semisubmersible.

Acknowledgments

The authors would like to appreciate Sabah Shell Petroleum Co. Ltd. for the financial support in preparing this paper.

References

- Bae, Y.H. and Kim, M.H. (2013), "Influence of failed blade-pitch-control system to FOWT by aero-elastic-control-floater-mooring coupled dynamic analysis", *Ocean Syst. Eng.*, **3**(4), 295-307.
- Bian, S. and Xiang, S. (2013), "Manage tensioner stroke for dry tree semisubmersible", *Proceedings of the 32nd International Conference on Ocean, Offshore and Arctic Engineering*, Nantes, France, June.
- Crotwell, G. and Yu, A. (2011), "Pull-style tensioner system for a top-tensioned riser", *U.S. Patent*: 8,021,081

- B2, issued Sep. 20, 2011.
- Gallagher, C., Williams, D. and Lang, D. (2012), "Modelling of marine riser tensioner load variations and implications for minimum top tension settings in drilling risers", *Proceedings of the 31st International Conference on Ocean, Offshore and Arctic Engineering*, Rio de Janeiro, Brazil, June.
- Grønevik, A. (2013), "Simulation of drilling riser disconnection - recoil analysis", M.Sc. Thesis, Norwegian University of Science and Technology, Trondheim.
- Haaland, S.E. (1983), "Simple and explicit formulas for the friction factor in turbulent pipe flow", *Fluid. Eng.*, **105**(1), 89-90.
- Kang, H.S. (2015), "Semi-active magneto-rheological damper and applications in tension leg platform / semi-submersible", Ph.D. Dissertation, Texas A&M University, College Station.
- Kang, H.S., Kim, M.H., Bhat Aramanadka, S.S. and Kang, H.Y. (2013), "Semi-active magneto-rheological damper to reduce the dynamic response of top-tension risers", *Proceedings of the 23rd International Offshore and Polar Engineering Conference*, Anchorage, USA, June.
- Kang, H.S., Kim, M.H., Bhat Aramanadka, S.S. and Kang, H.Y. (2014), "Dynamic response control of top-tension risers by a variable damping and stiffness system with magneto-rheological damper", *Proceedings of the 33rd International Conference on Ocean, Offshore and Arctic Engineering*, San Francisco, USA, June.
- Kang, H.Y. and Kim, M.H. (2012), "Hydrodynamic interactions and coupled dynamics between a container ship and multiple mobile harbors", *Ocean Syst. Eng.*, **2**(3), 217-228.
- Kim, S.J. and Kim, M.H. (2015), "Dynamic behaviors of conventional SCR and lazy-wave SCR for FPSOs in deep water", *Ocean Eng.*, **106**, 396-414.
- Koo, B.J., Kim, M.H. and Randall, R. (2004), "The effects of nonlinear multi-contact coupling with gap between risers and guide frame on global spar motion analysis", *Ocean Eng.*, **31**(11-12), 1469-1502.
- Koos, J. (2013), "Long stroke ram-style tensioner technology", *Proceedings of the Offshore Technology Conference*, Houston, USA, May.
- Kozik, T.J. (1975), "An analysis of a riser joint tensioner system", *Proceedings of the Offshore Technology Conference*, Houston, USA, May.
- Kozik, T.J. and Noerager, J. (1976), "Riser tensioner force variations", *Proceedings of the Offshore Technology Conference*, Houston, USA, May.
- Lee, C.-H. and Newman, J.N. (1991), "First-and second-order wave effects on a submerged spheroid", *Ship Res.*, **35**(3), 183-190.
- Leverette, S., Bian, X. and Rijken, O. (2013), "Dry tree semisubmersibles for Gulf of Mexico", *Proceedings of the Offshore Technology Conference*, Houston, USA, May.
- Li, S., Campbell, M., Howells, H. and Orsak, J. (2013), "Tension loss of hydro-pneumatic riser tensioners", *Proceedings of the 32nd International Conference on Ocean, Offshore and Arctic Engineering*, Nantes, France, June.
- Manring, N. (2005), *Hydraulic Control Systems*, Wiley, New Jersey, USA.
- Mathworks (2009). SimHydraulics Reference 1.5, The Mathworks Inc.
- Poll, P., Zou, J., Shi, S. and Kurup, N. (2013), "An evaluation of strength, fatigue and operational performance of dry tree semisubmersible riser tensioning equipment", *Proceedings of the Offshore Technology Conference*, Houston, USA, May.
- Ran, Z. (2000), "Coupled dynamic analysis of floating structures in waves and currents", Ph.D. Dissertation, Texas A&M University, College Station.
- Sten, R., Hansen, M.R., Larsen, C.M. and Sævik, S. (2010), "Force variations on heave compensating system for ultra-deepwater drilling risers", *Proceedings of the 29th International Conference on Ocean, Offshore and Arctic Engineering*, Shanghai, China, June.
- Trent, D. (2012), "Tensioner system with recoil controls", *U.S. Patent*: 8,157,013 B1, issued Apr. 17, 2012.
- Van de Ven, J.D. and Li, P.Y. (2009), "Liquid piston gas compression", *Appl. Energy*, **86**(10), 2183-2191.
- Xiang, S., Cao, P., Otten, J., Jiang, L. and Bian, S. (2014), "Top tensioned riser interface with dry-tree semisubmersible", *Proceedings of the 33rd International Conference on Ocean, Offshore and Arctic Engineering*, San Francisco, USA, June.

- Yang, C.K. (2009), "Numerical modeling of nonlinear coupling between lines/beams with multiple floating bodies", Ph.D. Dissertation, Texas A&M University, College Station.
- Yang, C.K. and Kim, M.H. (2010), "Linear and nonlinear approach of hydropneumatic tensioner modeling for Spar global performance", *Offshore Mech. Artic Eng.*, **132**(1), 011601.
- Yang, C.K. and Kim, M.H. (2011), "The structural safety assessment of a tie-down system on a tension leg platform during hurricane events", *Ocean Syst. Eng.*, **1**(4), 263-283.
- Zeng, Y., Wanvik, L-G., Wang, T., Rasmussen, S. and Lu, R. (2013), "Dry-tree semi-submersible production and drilling unit", *U.S. Patent Application Publication*: US 2013/0032076 A1, issued Feb. 7, 2013.